Cu Nanodendrite Foams on Integrated Band Array Electrodes for the Nonenzymatic Detection of Glucose

Vuslat Juska, Alain Walcarius, Martyn Pemble

Cu Foam Nanostructures on Integrated Band Array Electrodes for the Non-Enzymatic Detection of Glucose

Vuslat Buk[1, 2]*, Alain Walcarius[3] and Martyn E. Pemble[1, 2]
[1]School of chemistry, University College Cork, Cork, IRELAND
[2]Tyndall National Institute, Lee Maltings Complex, Dyke Parade, Cork, IRELAND
[3]Laboratoire de Chimie Physique et Microbiologie pour les Matériaux et l'Environnement (LCPME), UMR 7564, CNRS-Université de Lorraine, 405 rue de Vandoeuvre, 54600 Villers-les-Nancy, France

Abstract:

We demonstrate the successful electrodeposition of Cu nanodendrite foams onto a series of lithographically formed gold band electrodes at negative overpotentials (-5V and -6V) in an acidic environment. The nanodendrite foams were deposited onto two different integrated microelectrode arrays fabricated using standard lithographic techniques. Each electrode consisted of 17 gold band electrodes deposited onto a silicon wafer substrate, labelled BA5 (with a width of 5 μm and a length of 250 μm) and BA10 (with a width of 10 μm and a length of 500 μm). Prior to Cu deposition the gold electrodes were characterized by scanning electron microscopy (SEM) in order to evaluate the morphology of each design and by cyclic voltammetry (CV) in order to investigate their diffusion profiles. After Cu deposition the resulting 3D foam structures were studied using SEM, XPS and EDX. The Cu foam/Au microelectrodes were then used for the electrocatalytic detection of glucose via oxidation at a potential of +0.45 V vs. Ag/AgCl in an alkaline medium. It was found that both types of electrode arrays used showed excellent analytical performance in terms of sensitivity, reproducibility and stability in comparison with the best performances reported in the literature. In particular, the BA5-CuFoam electrode exhibited an outstanding sensitivity of 10,630 μA mM^{-1} cm^{-2} towards glucose with a wide linear range up to 22.55 mM. The performance of this new type of electrochemical sensor is attributed to a combination of the use of the very high surface area Cu nanodendrite foam and the enhanced radial distribution profile associated with the use of the smaller band microfabricated electrodes. Additionally, both biosensors also showed a strong resistance to the poisoning effects of chlorine ions and excellent stability over a period of three months.

Key words: microfabrication, band array electrode, electrocatalysis, copper nanodendrites

Introduction:

Besides the reproducibility and low variability of silicon-based microelectrodes, their use allows for flexibility in the design and arrangement of the array with numerous shapes, sizes and dimensions available for each electrode on the array[1,2]. Furthermore, precise batch fabrication may provide a cost effective solution for all the fabrication processes. In particular, the use of silicon based micro electrodes as neural probes in the field of neural science for *in vivo* recordings and/or implantable (bio) sensors have been extensively reported since silicon, along with the often applied silicon dioxide and silicon nitride insulator layers, is a biocompatible material[1,3-6]. For example, the research article by Wei et al.[7] describes an important example of the use of implantable silicon based microelectrode arrays (MEAs) for L-glutamate detection, which is the most common excitatory neurotransmitter for a wide range of neurological diseases. The developed MEA was capable of detecting glutamate with a sensitivity of 56 pA μM^{-1} and a detection limit of 0.5 µM. Furthermore, this study successfully demonstrated the results of monitoring the extracellular glutamate levels, spikes and local field potentials *in vivo*. Micro- or nano-sized silicon based micro fabricated electrodes have also been of great interest for (bio) electrochemical applications[8,9]. From the electrochemistry perspective, the scaling down of the electrodes approach has been reported by many researchers[10-13] who have demonstrated the benefits of using these small electrodes in terms of the electro-analytical performance including sensitivity and detection limit.

In a previous study, we demonstrated the positive advantage of using micron-sized array electrodes by developing glucose oxidase (GOx) biosensors based on both planar[9] and micro array electrodes[8] with sensitivities of 47.24 and 626.06 µA mM^{-1} cm^{-2}, respectively. The observation of a 13-fold improvement of the sensitivity resulting from the move from planar to micro array electrodes clearly highlighted the advantages of successfully miniaturizing the developed biosensor.

Another potential way to enhance the performance of a glucose sensor is to utilize the electro-oxidation of glucose which requires a catalyst such as platinum, gold, copper or cobalt, instead of employing an enzymatic reaction[14-17]. Among the possible catalytic metals copper (Cu) - a 3d transition metal - is considered to be a highly promising candidate for many applications in nanotechnology since Cu-based nanomaterials can promote and undergo a variety of reactions due to the presence of two accessible oxidation states which enable reactivity via both one- and two-electron pathways[18].

Cu based nanocrystals have found many applications in electrocatalysis[19], photocatalysis[20], biosensors[21] and electrochemical sensors[22]. The morphology of the Cu-based nanoparticles on the solid electrode surface has a great impact on the catalytic reaction of glucose. The size and shape of these nano structures is highly dependent on the synthesis approach and precursors used. For instance, a variety of copper[23], cupric oxide[24], cuprous oxide[25] nanomaterials with different sizes and shapes, often in combination[26] have been used to prepare non-enzymatic sensors and have demonstrated a high sensitivity towards glucose. The most remarkable advantage of those sensors is the increased stability which has been observed, since stability represents the biggest problem for enzymatic sensors due to the nature of the biomolecule itself. However, until now, CuFoam deposited micro fabricated band array electrodes have not been investigated for glucose electro-oxidation.

In this present work we demonstrate the excellent performance of CuFoam micro band array electrodes for glucose oxidation. We show that CuFoam formed in an acidic environment via negative overpotential deposition exhibit well-ordered porous electro-active surfaces for the electrocatalytic detection of glucose. The resulting sensors showed superior electro-analytical performance as a result of the reduction in geometric surface area of each design combined with the increased electro-active surface area of the porous CuFoam. The morphologies of the bare and modified electrodes were studied with scanning electron microscopy (SEM). Gold band array electrodes with different widths and lengths were microfabricated on a silicon substrate by applying deposition, lithography and etching and were then characterized electrochemically by applying cyclic voltammetry (CV). CuFoam nanostructures were

electrochemically grown on the array electrodes in an acidic environment at high negative overpotentials in order to obtain foam shaped porous deposition layer.

The sensors developed here showed excellent performance even in the presence of the chloride ions and other potentially interfering species. Furthermore, the micro array electrodes exhibited large linear ranges and showed considerably better sensitivities towards glucose than electrocatalytic sensors available in the literature, please see Table 2.

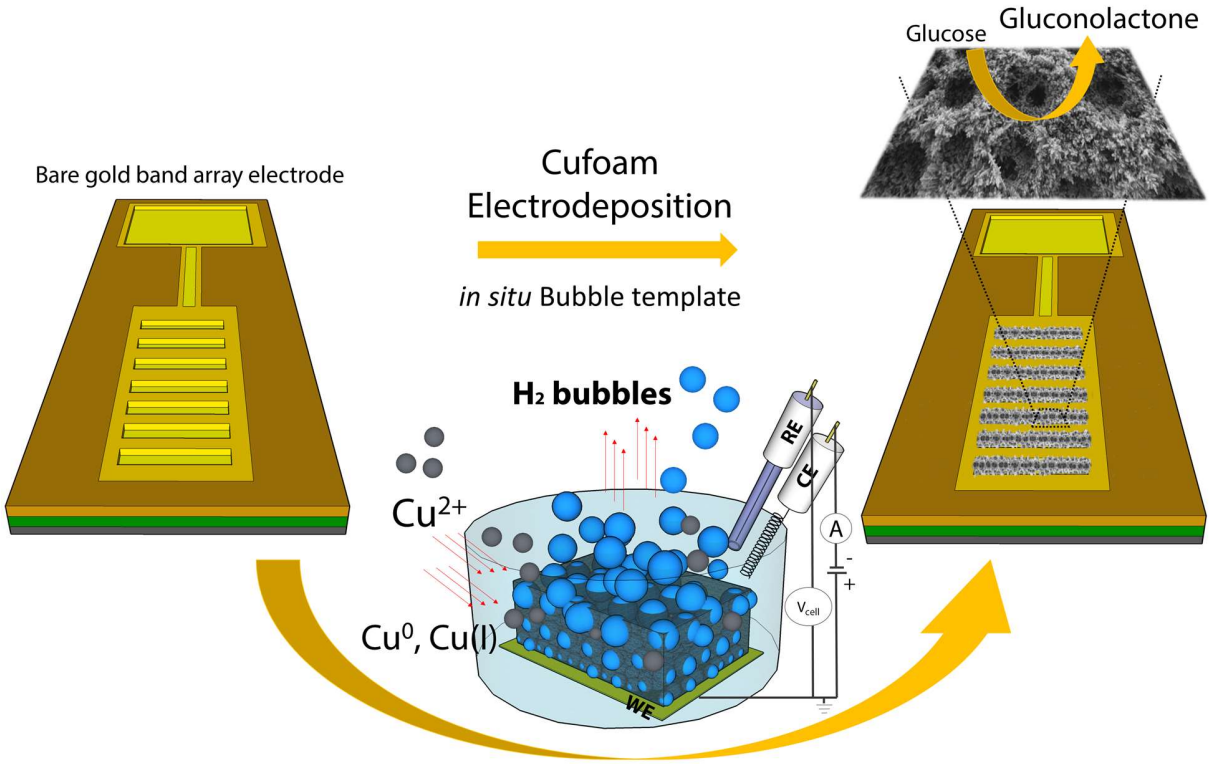

Scheme 1. Schematic illustration of *in situ* bubble template formation and copper foam electrodeposition onto microfabricated band array electrode

Results and discussion

Fabrication and investigation of gold micro band array electrodes

In this section we describe the lithographic fabrication of two different geometrical types of microelectrode arrays consisting of 17 gold band electrodes placed on top of a silicon wafer substrate. The silicon fabrication process included oxide layer growth on the silicon substrate after a series of cleaning steps of the substrate. **Table 1** summarizes the two different band array geometries fabricated and studied here. Electrodes were fabricated in several process steps by lithography, deposition and etching as described previously[9] with a specific mask having been designed for the band array electrodes. This was followed by dicing to separate each electrode. To evaluate the success or otherwise of the fabrication process we performed detailed characterization of clean, bare micro array electrodes, as described below.

The arrangement, size and dimensions of the bare electrodes were analyzed by scanning electron microscopy (SEM). As can be seen in Fig. 1A and B, SEM micrographs clearly show the arrangement of the 17 individual band electrodes that are arranged on the Si_3N_4 insulation layer with 100 µm inter electrode

distance between electrodes. Fig. 1C shows a higher magnification image of electrode array BA5 with a width of 5 µm and a length of 250 µm, placed at 100 µm inter electrode distance. Fig. 1D shows a higher magnification image of electrode BA10 had a width of 10 µm and a length of 500 µm, placed at 100 µm inter electrode distance. Each design of the array electrodes consisted of an isolated connection track and an etched large surface area connection pad, as illustrated in Fig. 1G.

For the initial electrochemical characterization of the bare gold electrodes cyclic voltammetry (CV) was performed in the presence of the redox probe $Fe(CN)_6^{3-/4-}$ in 0.01 M PBS, containing 0.1 M KCl. As shown in Fig. 1E, BA5 exhibits a sigmoidal voltammogram which is characteristic behavior for most microelectrodes. However, in Fig. 1 F, BA10 shows a voltammogram which displays the characteristic peaks associated with a conventional reversible redox couple. While each band array design has the same inter electrode distance, the increased (×2) width and length of BA10 may result in an increased diffusion profile diameter which then creates an overlapping diffusion zone between the adjacent band electrodes. Thus, BA10 shows a characteristic voltammogram shape which is a combination of that expected for both planar electrodes and microelectrodes. Representative diffusion profiles are shown as inset graphs of Fig. 1E and F. Moreover, BA10 displays increased current levels in comparison to BA5, which may attributed to increased total surface area with increased number of the electrodes on the array, **Table 1**.

Table 1. Characteristics of the micro band array electrodes

BAND	Width (µm)	Length (µm)	Inter electrode distance (µm)	Electrodes	Recess depth (nm)	Geometric surface area (cm^2)
BA5	5	250	100	17	200	2.13×10^{-4}
BA10	10	500	100	17	200	8.50×10^{-4}

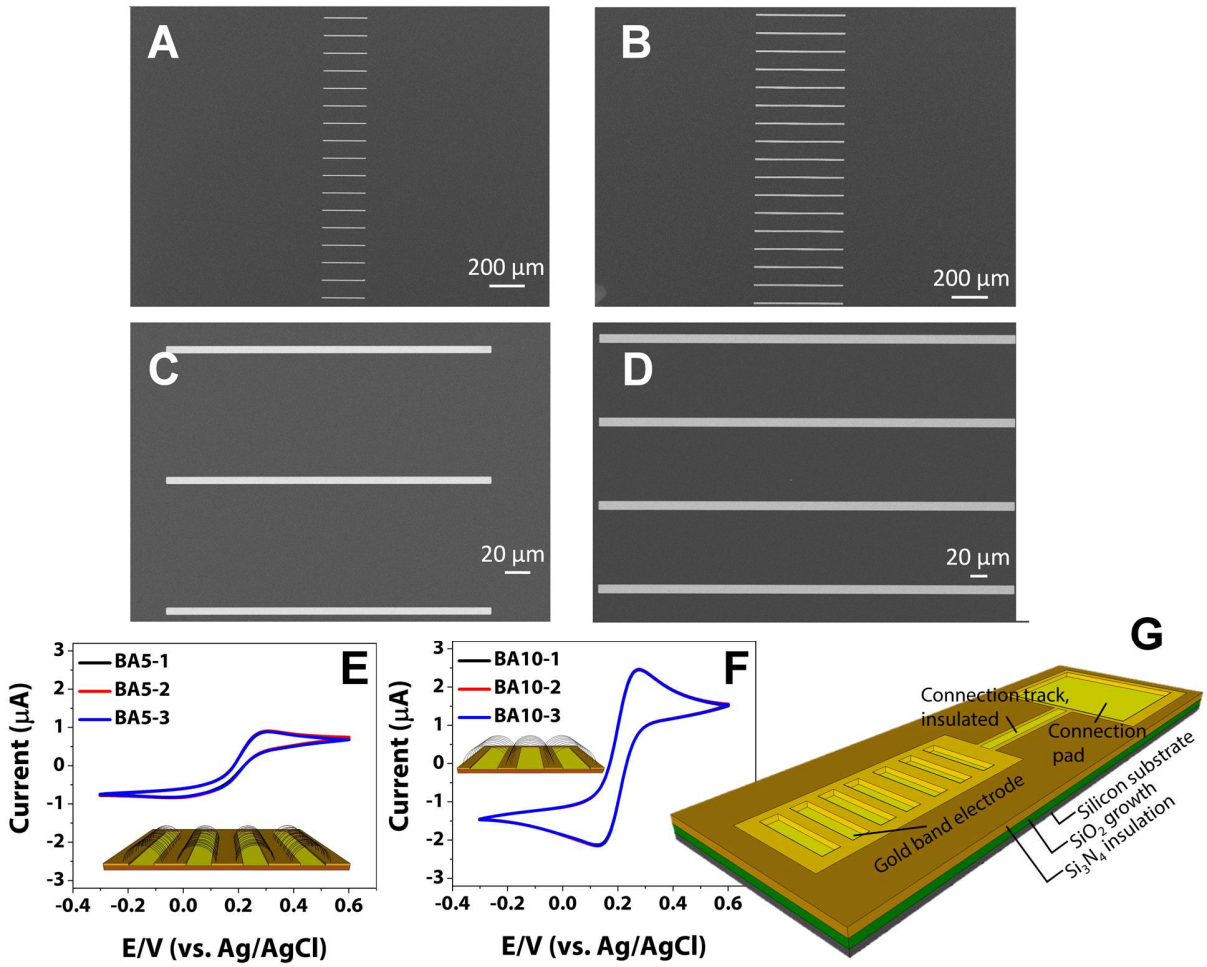

Figure 1. SEM images of gold band array electrodes; lower magnification images of BA5 (A) and BA10 (B), higher magnification images of the band electrodes of BA5 (C) and BA10 (D), cyclic voltammograms recorded for BA5 (E) and BA10 (F) at a scan rate of 0.01 V s^{-1}. The solution is 5 mM $Fe(CN)_6^{3-/4-}$ as a redox probe in 0.01 M PBS (pH 7.4), containing 0.1 M KCl, each design repeated 3 times (inset pictures are the representative images of diffusion profiles of BA5 and BA10, not drawn to scale). Illustration of the band array electrode (not drawn to scale) (G).

Electrodeposition of CuFoam and electrocatalytic behavior of CuFoam deposited band array electrodes

CuFoam modified band arrays were prepared by electrodeposition using a condition that can concurrently reduce water to H_2. The H_2 bubbles formed on gold working electrode served as an *in situ* generated bubble template to deposit porous CuFoam[27,28], as illustrated in **Scheme 1**.

Nikolic et al.[29] studied in detail the effect of the H_2SO_4 concentration over the morphology of Cu deposits by keeping the concentration of Cu^{2+} constant in the solution. In our study, the acidity of the solution also played a crucial role in the formation of well-ordered 3D roll-shaped CuFoam deposits over each gold band electrodes. We studied concentrations of H_2SO_4 of 1 M (Fig. 2A), 0.5 M (Fig. 2B) and 0.05 M (Fig. 2C) to demonstrate the effect of acidity while the Cu^{2+} concentration was kept constant**.** With decreased acid concentrations, we observed a decrease in the thickness of the Cu dendrites. In the case of the 0.05M H_2SO_4 concentration, we observed random deposits over the electrode surface with the needle-shaped fragile Cu dendrites which were weakly attached to the surface (**Fig. 2C**). This result shows the acidity of

the electrodeposition solution has an important impact on the adhesion of Cu nanocrystals on the gold electrode surface.

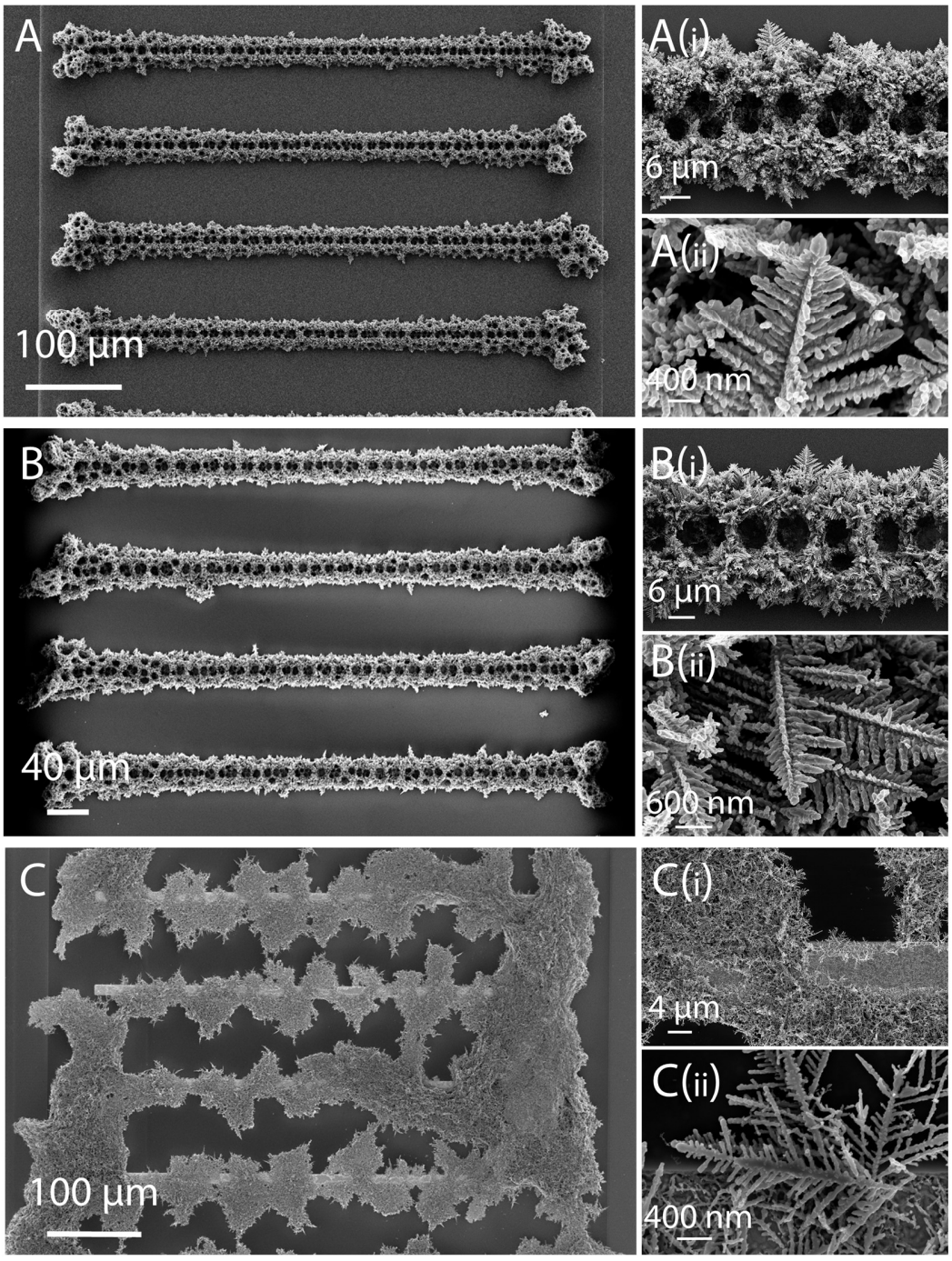

Figure 2. SEM images of BA10-CuFoam electrodes prepared at different H_2SO_4 concentrations; (A, A-i and A-ii; increased magnification), 1M H_2SO_4, (B, B-i and B-ii; increased magnifications) 0.5M H_2SO_4, (C, C-i and C-ii; increased magnifications) 0.05M H_2SO_4at a applied voltage of -6 V vs. Ag/AgCl in the solution containing 0.87 mg Cu^{2+}

As might be expected, the use of shorter deposition periods led to a decrease in the density of the CuFoam deposits over the band electrode surface. **Fig. S1** shows the SEM micrographs of BA10-CuFoam electrodes which were prepared after 15, 20, 30 and 35 seconds of electrochemical deposition**.** Due to the microelectrode diffusion characteristics, we observed that the Cu deposits became denser only at the ends of the each band electrode in the array at shorter deposition times and with increased deposition time we obtained a more uniform foam distribution through the middle of the single band electrode. However, for each design of band array electrode, we obtained a denser accumulation of the Cu dendrites at the both ends of the electrodes and the diameter of the pores in the copper deposits was found to increase towards the outer surfaces of the deposits. Moreover, it was found that applied voltage also had a significant impact on the nature of the deposits along each band electrode, **Fig. S2.** Therefore, in the presence of a suitable concentration of ions, using an optimized applied potential and deposition time as explained in the experimental section, Cu dendrites were grown in the interstitial spaces of the dynamic hydrogen bubble template which was generated in situ on the working electrode, the result being the formation of a microporous 3D CuFoam on the surface[27,30], as illustrated in Scheme 1. The resulting optimum Cu dendrites were grown at high concentration of SO_4^{2-} and high negative overpotentials of -5.0 and -6.0 V vs. Ag/AgCl in the case of BA5 and BA10, respectively. Fig. 3A and B show the 3D CuFoam deposited onto BA5 and BA10, respectively. The wall of the CuFoam deposits is composed of dendritic nanostructures resulting in the increased surface area as can be seen in the higher magnification of SEM micrographs of both electrodes, Fig. 3C, D, and E.

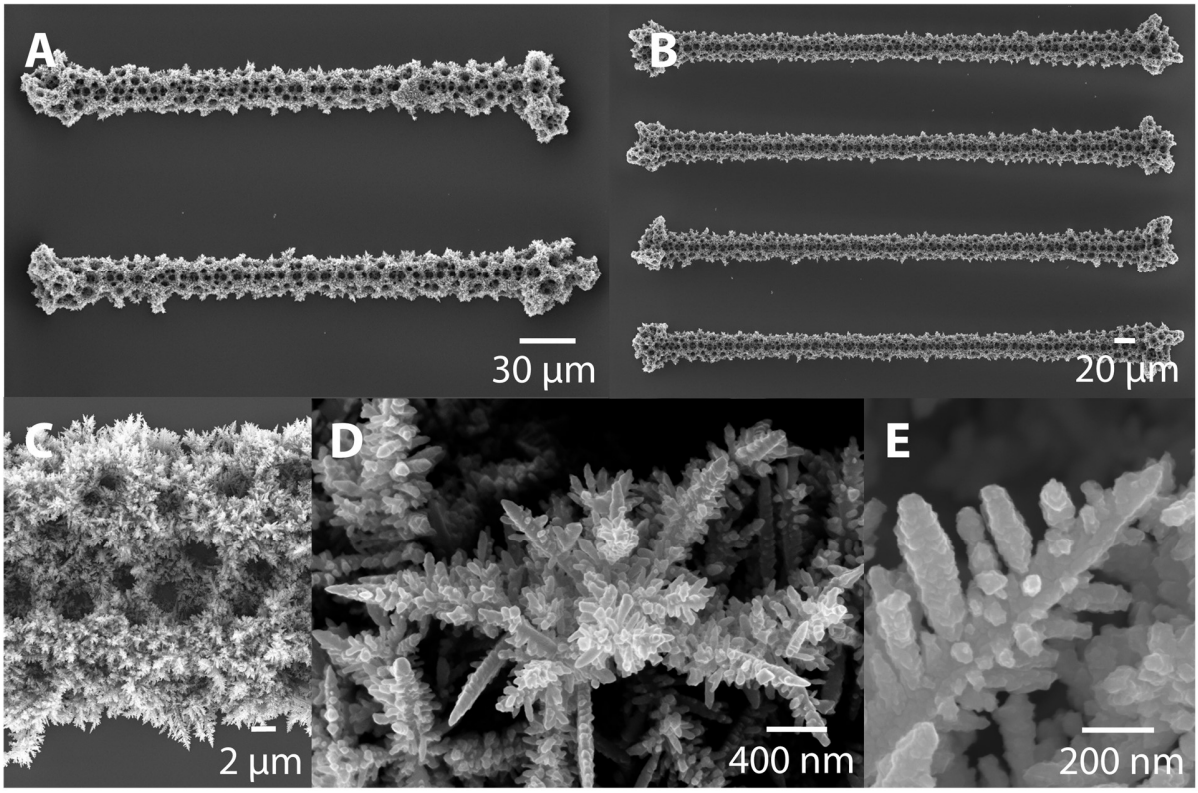

Figure 3. SEM images of CuFoam band array electrodes showing (A) BA5 and (B) BA10 foam structure, (C) porous foam of single band and (D and E) foam wall and dendritic Cu nanostructures at higher magnifications.

The as-prepared CuFoam band array electrodes were used to investigate glucose electro-oxidation. **Fig. 4A** shows the electrochemical behavior of the CuFoam band array electrode in an alkaline solution and Fig.4B and C show the changes of the voltammograms in the absence and presence of glucose. In the anodic sweep in 0.1 M NaOH solution (**Fig. 4A**), the first multiple peaks observed at around -0.04 V vs Ag/AgCl may attributed to oxidation of Cu(0) to Cu(I) and the subsequent formation of Cu_20, according to following equation[31-33];

$$2\,Cu^0 + 2\,OH^- \rightarrow\ Cu_2O + H_2O + 2\,e^- \quad (1)$$

The broad peak at around 0.13 V vs Ag/AgCl may be attributed to further oxidation of Cu(I) to Cu(II) and Cu(0) to Cu(II), according to following equations [32];

$$Cu_2O + 2\,OH^- \rightarrow\ 2CuO + H_2O + 2\,e^- \quad (2)$$

$$Cu_2O + 2\,OH^- + H_2O \rightarrow 2Cu(OH)_2 + 2\,e^- \quad (3)$$

In the cathodic sweep, the peak at around -0.52 V is the reduction of copper oxide species. After addition of glucose into the electrochemical cell (**Fig. 4B and C**, red lines), both electrodes give rise to voltammograms that show the electro-oxidation potential of glucose at +0.45 V vs Ag/AgCl while there are no other obvious peaks at the same potential in the absence of the glucose. The most possible explanation for the glucose-electro-oxidation in NaOH solution by Cu has been postulated as the formation of Cu(III) oxides (such as CuOOH). During the cyclic voltammetry scanning, the exterior surface of the foam is oxidized to CuO and further to Cu^{3+} which is rapidly reduced to Cu(II) at 0.64 V vs Ag/AgCl [34-36];

$$Cu(II) \rightarrow\ Cu(III) + e^- \quad (4)$$

$$Cu(III) + 4\,OH^- \rightarrow\ Cu(II) + 2H_2O + O_2 \quad (5)$$

$$Cu(II) - \text{glucose} \xrightarrow[-e^-]{} Cu(III) - \text{glucose} \xrightarrow[-e^-]{} \text{Gluconolactone} + Cu(II) \quad (6)$$

As the aim of the present work was to study the oxidation of the glucose, +0.45 V vs Ag/AgCl was selected as the potential for use in the subsequent analytical studies.

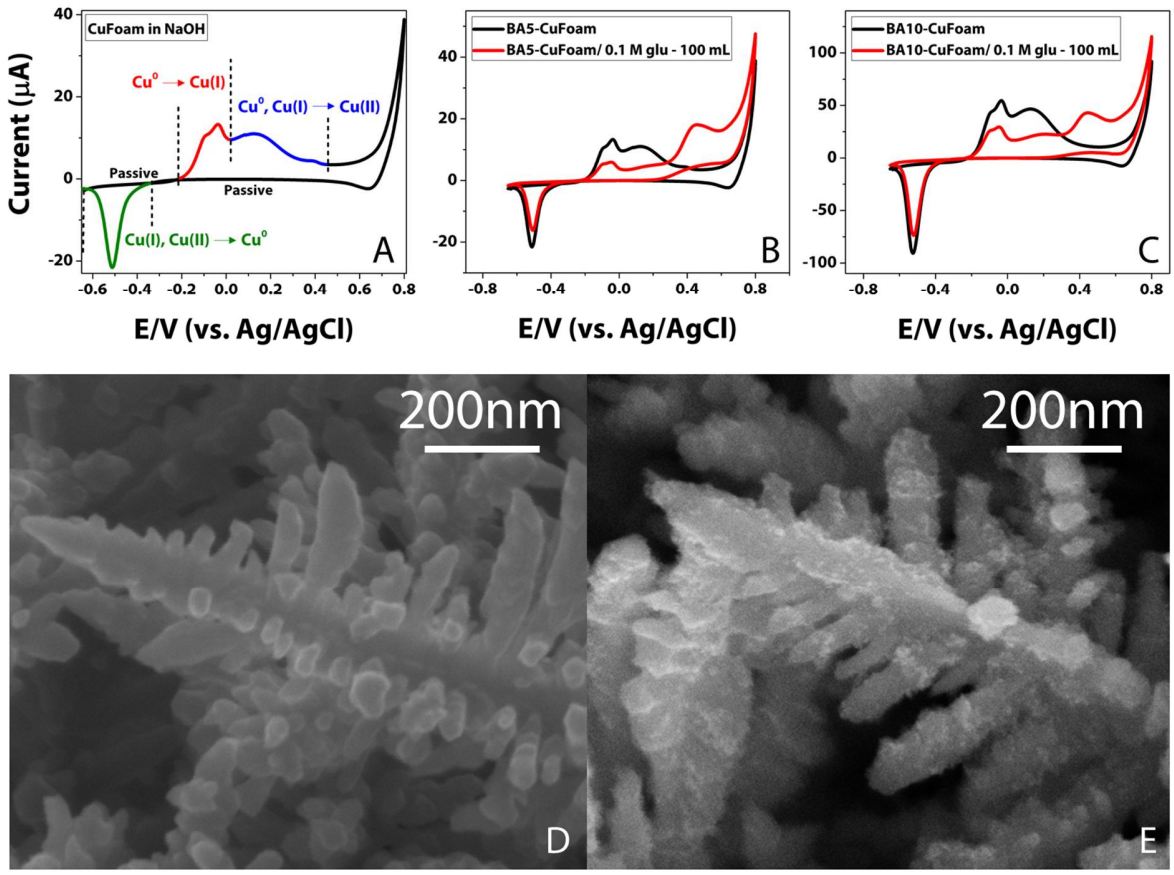

Figure 4. Cyclic voltammogram of CuFoam electrode in 0.1M NaOH solution (A), Cyclic voltammograms of the BA5-CuFoam (B) and BA10-CuFoam (C) microelectrodes in 0.1 M NaOH (black), and in the presence of 2 mM glucose (red), at a scan rate of 0.01 V s^{-1}, SEM images of the deposited Cu nanostructure before (D) and after (E) glucose electro oxidation.

Fig. 4D shows a high magnification SEM image of the CuFoam dendritic nanostructure. The CuFoam structure and Cu dendrites remained stable after electro-oxidation of glucose (**Fig. 4E**). However, the surface roughness changed with the appearance of the very small spike-like features over the surface of Cu dendrites (**Fig. 4E**). Those small features may be responsible for the catalytic performance of the CuFoam electrodes[27]. Nam et al. [27] observed very similar features appearing over a CuFoam surface after the electrochemical oxidation of 5-hydroxymethylfurfural. They claimed that these spike-like features covering the surface of Cu crystals were composed of similar amounts of CuO and $Cu(OH)_2$ on the surface which was demonstrated with X-ray photoelectron spectroscopy (XPS) results. Indeed, it has been reported that the electrocatalytic oxidation of glucose on copper electrodes happens via copper oxide/hydroxide intermediates[37-39]. Therefore, the surface chemical composition of the CuFoam electrodeposits before and after glucose electro-oxidation was studied by analyzing Cu 2p peaks obtained by XPS. Fig 5A shows the measured and fitted curves of CuFoam deposits and Fig. 5C exhibits the whole survey of the surface presents all the elements detected. Due to the existence of only C (from atmosphere), O and Cu, it suggests that only copper oxides were formed on the surface. High resolution spectra of Cu 2p (Fig. 5A) reveals clearly that indeed a mixture of elemental copper and copper-oxide species are present on the surface. The peaks located at approximately 932.6 and 952.5 eV were attributed to Cu_2O and Cu^0. The peaks at 954.6 eV and 934.9 eV were assigned to CuO and $Cu(OH)_2$,

respectively. **We remark the limitation of the XPS analysis of the surface layer, because the Cu 2p peaks of Cu^+ and Cu^0 cannot be differentiated, which means that the Cu_2O peak may include the peak from the underlying elemental copper lies beneath the copper oxides surface layer[27].** After the electro-oxidation of glucose, the surface of the CuFoam electrode was reexamined with XPS. The whole survey shows clearly that the surface of the CuFoam deposits are still composed of a mixture of copper oxide species, Fig. 5D. However, the high resolution spectra of the foam surface demonstrates the significant changes of the composition of the existing species (Fig. 5B). The peak at 932.6 eV attributed to Cu^+/Cu^0 decreased significantly and the Cu^{2+} at 934.9 eV increased. Similarly, the peak of Cu^{2+} (CuO) at 954.3 eV was increased, while the peak of Cu^+ at 952.5 eV decreased. The increase of the Cu^{2+} species – $Cu(OH)_2$ and CuO- is most likely due to the result of reduction of CuOOH to Cu^{2+} after the electro oxidation of glucose, Eqs. 2, 3 and 6.

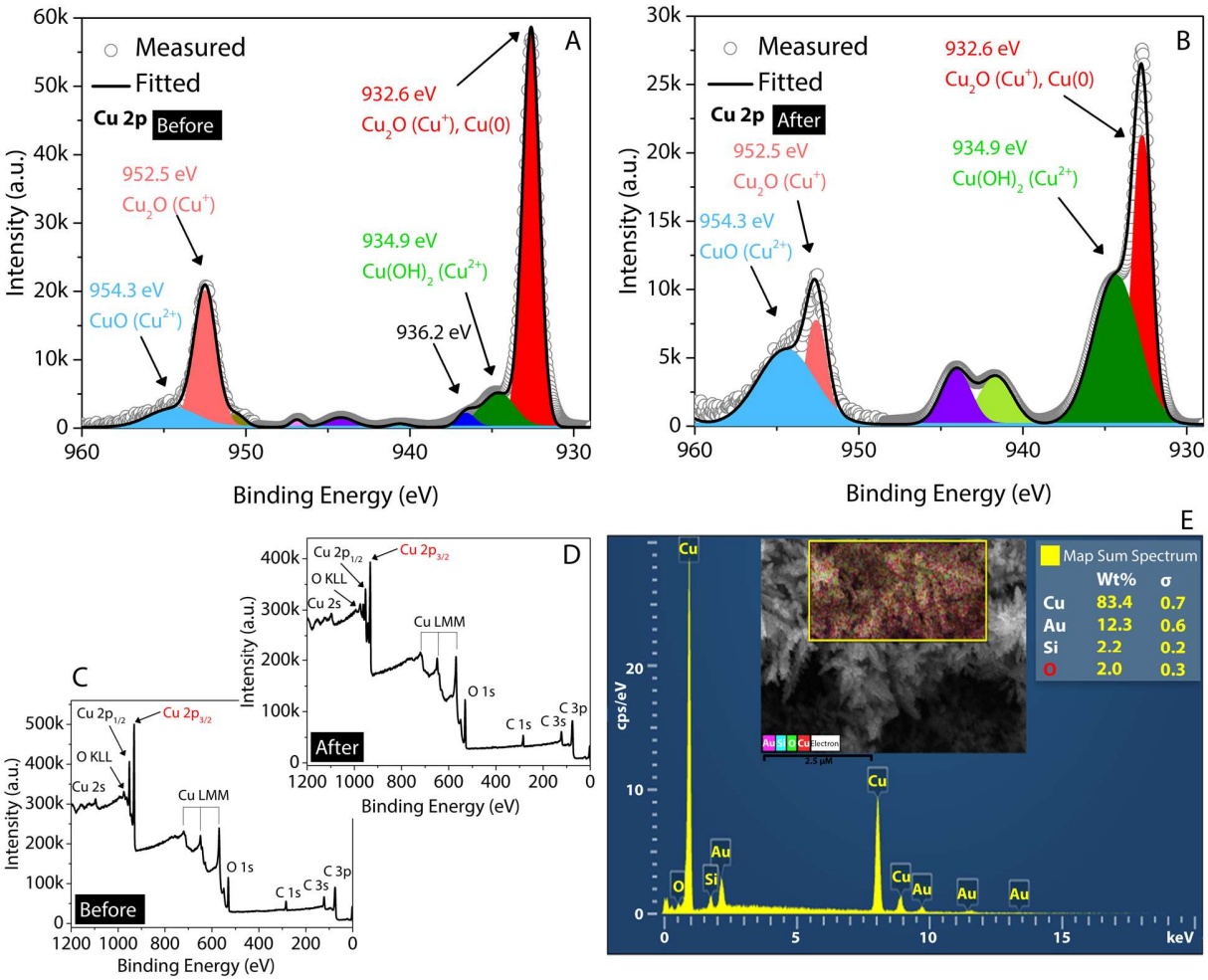

Figure 5. Cu 2p XPS spectra of CuFoam deposits (A) before and (B) after glucose electro-oxidation, XPS survey scans of CuFoam (C) before and (D) after glucose electro-oxidation (**The quantification results of high resolution spectras are shown in Table S1**) and (E) EDX spectra of CuFoam electrodeposits

The other technique used in here to analyze the chemical structure of the CuFoam electrodes is the energy-dispersive X-ray spectroscopy (EDX). Fig. 5E shows the EDX analysis and corresponding mapped

SEM image of the analysis. The copper appears by red colour which covers the entire surface or the analysis area with the ratio of % 83.4. The result of the EDX analysis confirms the copper and copper oxides as the main constituent in the structure in the presence of gold (Au) and silicon (Si). These two elements are presented less corresponds to the existence of the electrode material based on silicon and gold.

To demonstrate the relationship between the concentration of deposited Cu crystals on surface and the sensitivity of the sensors, we measured calibration curves for the BA-CuFoam electrodes prepared using different Cu deposition times. The fittings of BA5-CuFoam with 20 seconds deposition time (■; $J(\mu A/cm^2) = 10{,}630\ [C_{glucose}](mM) + 53$, R^2=0.997), 15 seconds deposition time (●; $J\ (\mu A/cm^2) = 7136\ [C_{glucose}](mM) + 1284$, R^2=0.989), 10 seconds deposition time (▲; $J(\mu A/cm^2) = 6369\ [C_{glucose}](mM) + 17$, R^2=0.955) and the fitting equations of BA10-CuFoam with 25 seconds deposition time (■; $J(\mu A/cm^2) = 4437\ [C_{glucose}](mM) - 24$, R^2=0.999), 20 seconds deposition time (●; $J(\mu A/cm^2) = 3903\ [C_{glucose}](mM) + 6$, R^2=0.996), 15 seconds deposition time (▲; $J\ (\mu A/cm^2) = 2882\ [C_{glucose}](mM) + 41$, R2= 0.990) are given in Fig. 6A and B as calibrations curves for each deposition times. As expected, lower Cu deposition times produced electrodes that showed decreased sensitivity due to a decrease in the electro-active surface area. Furthermore we observed a decreased correlation coefficient for electrodes grown with decreased Cu deposition time since the sensors' saturation levels decreased. In this regard it was found that for the BA5 electrodes growth of less than 20 seconds resulted in a marked decrease in both sensitivity and dynamic range for glucose detection, while for the BA10 electrodes this critical growth period was 25 seconds.

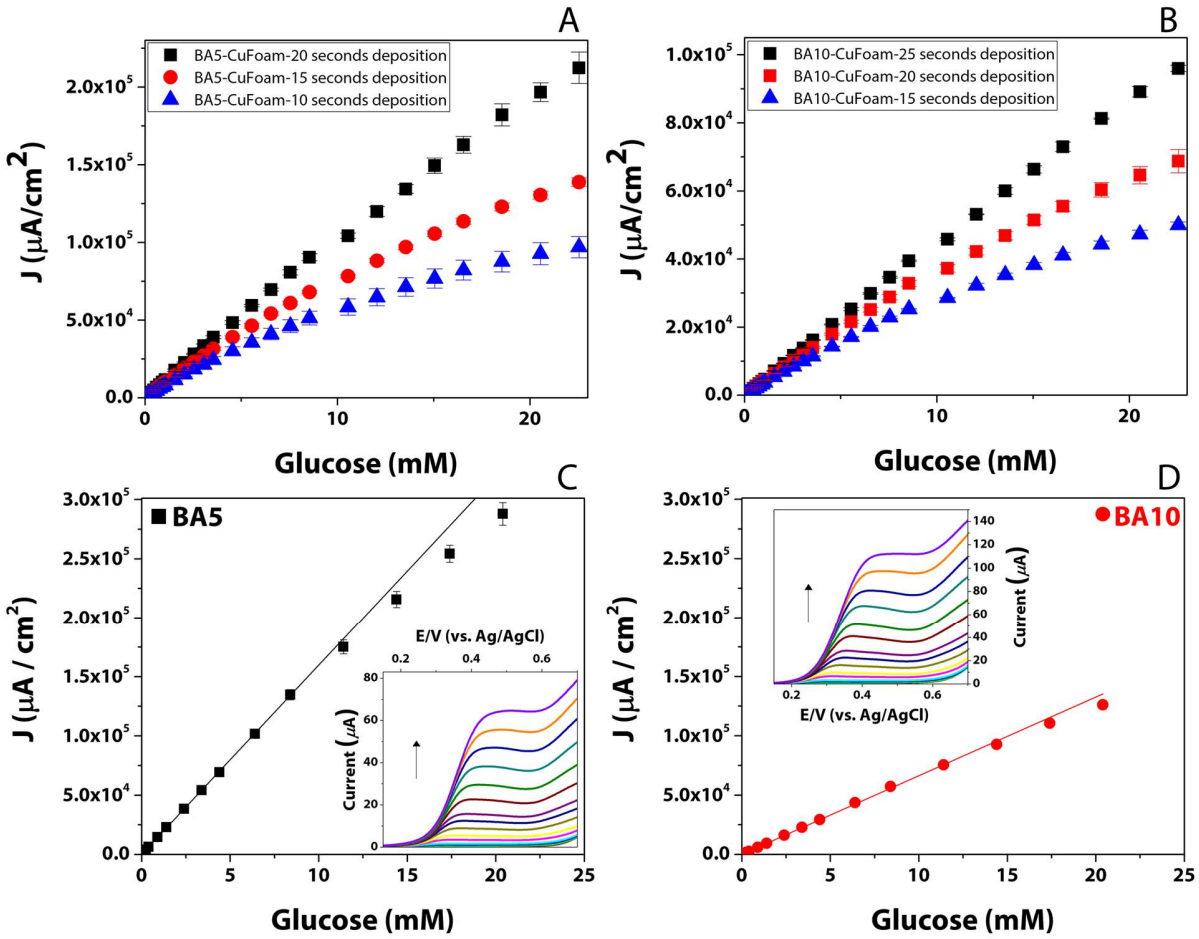

Figure 6. Calibration curves of BA5-CuFoam (A) and BA10 with 20 seconds (■), 15 seconds (●), and 10 seconds (▲) deposition times, illustrating the linear relationship observed between glucose concentration and current density for BA5-CuFoam (C) and BA10-CuFoam (D) biosensors with a correlation co-efficient R^2=0.99 for both electrodes and linear sweep voltammograms of BA5-CuFoam (C-inset) and BA10 (D-inset) biosensors in 0.1 M NaOH towards increase concentration of glucose at a scan rate of 0.01 V s^{-1}

The linear sweep voltammograms (LSV) obtained as a function of increasing glucose concentration over the CuFoam deposited BA5 and BA10 electrodes are shown in **Fig.6 Cand D.** The anodic peak at +0.45 V increases with increasing concentration of glucose as shown in inset graphs. While the peak shape is the same for both designs, the BA10-CuFoam array electrode exhibits higher current levels than the BA5-CuFoam array electrode. **Fig. 6C and D** reveal the corresponding glucose concentration vs. current density graph for the BA5 and BA10 electrodes, respectively. These obviously linear responses towards glucose demonstrate that the CuFoam deposited band array electrodes exhibit a uniform response to glucose and show excellent electrocatalytic behavior.

Chronoamperometric detection of glucose and analytical parameters of the CuFoam deposited array electrodes

The as-prepared CuFoam deposited band array electrodes were studied as glucose sensing anode materials. **Fig. 7A, B** shows the chronoamperometric responses and corresponding calibration curves of both the BA5 and BA10 electrodes modified by Cu deposition. Chronoamperometry was applied as a

function of increasing concentrations of glucose in 0.1 M NaOH solution at room temperature under non-stirred conditions. After each addition of glucose, the solution was stirred to obtain a homogenous distribution of glucose in the electrochemical cell and then kept stable for 15 seconds in order to reach equilibrium before the measurement. The inset graphs on **Fig. 7A, B** show the magnified images of six chronoamperograms. The current obtained at the 40th second was used to prepare the calibration curves. **Fig. 7C and D** show the corresponding calibration curves of BA5 and BA10 CuFoam biosensors, respectively. Both calibration curves exhibit a linear region in the range of concentrations between 0.01 mM - 22.55 mM. The fitting equation of BA5, **Fig. 7C**, is $J\ (\mu A/cm^2) = 10{,}630\ [C_{glucose}](mM) + 54$ with a correlation coefficient of 0.997 and the fitting equation of BA10, **Fig. 7D**, is $J\ (\mu A/cm^2) = 4{,}437\ [C_{glucose}](mM) - 24$ with a correlation coefficient of 0.999. The slope of the calibration curves demonstrates the sensitivities of the BA5 and BA10 to be 10,630 µA mM^{-1} cm^{-2} and 4,437 µA mM^{-1} cm^{-2}, respectively. Both biosensors showed excellent sensitivities towards glucose in comparison to many other array- based sensors reported in the literature, **Table 2**. The increased sensitivity of BA5 in comparison to the sensitivity of BA10 is due to the further miniaturization of the array and the advanced microelectrode properties arising from the diffusion profile of the miniaturized electrode. This result clearly shows the positive advantage of the miniaturized systems in terms of the analytical performance of the desired (bio)-sensors.

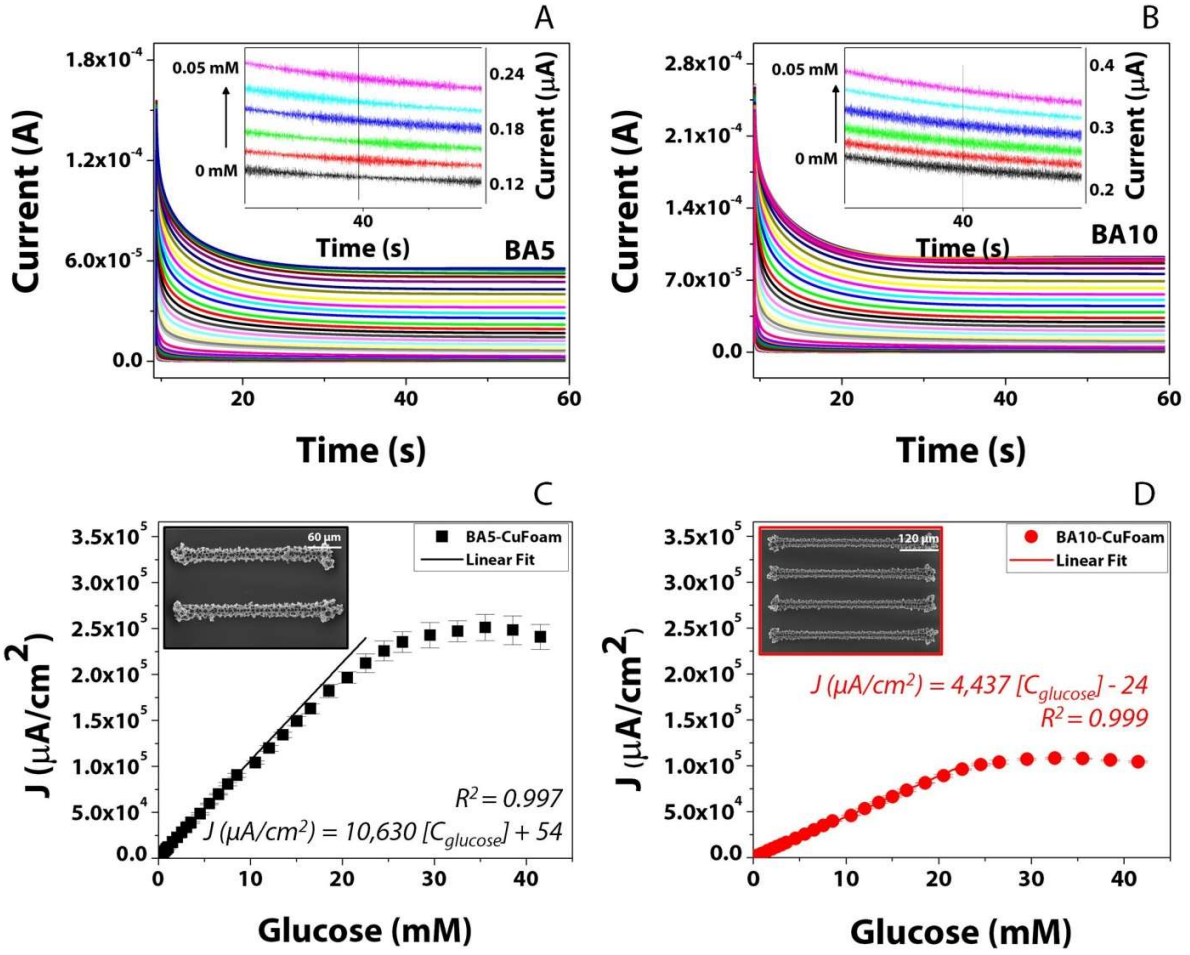

Figure 7. Chronoamperograms of the BA5-CuFoam (A) and BA10-CuFoam (B) biosensors obtained in 0.1 M NaOH solution as a function of increasing concentration of glucose at an applied potential of + 0.45 V

(inset graphs show the magnified image of first six chronoamperograms at 40th second), and corresponding calibration curves for the BA5-CuFoam (C) and BA10-CuFoam (D) biosensors.

Table 2 presents a summary comparison of the main characteristics of the array based non-enzymatic glucose sensors reported in the literature and the BA5, BA10 CuFoam sensors fabricated in this study. The biosensors developed in this study show the widest linear range for glucose detection up to 22.55 mM among all the array based sensors reported in **Table 2**. The sensitivity of BA5 CuFoam electrode is one of the highest sensitivity among the listed sensors. These performance characteristics may be attributed to the high quality fabrication of the array electrode with the smaller surface area of 2.13×10^{-4} cm^2. Hence it is proposed that the electrochemical characteristics of the designed electrode are highly suitable for the development sensors or biosensors. The relatively easy, one-step deposition of 3-D structured porous CuFoam onto the band array electrode provides very a large electro-active surface area for glucose oxidation with superior sensitivity of 10,630 µA mM^{-1} cm^{-2}. As discussed earlier (Fig. S3), the increased concentration of the Cu nanocrystals on the surface, facilities the enhancement of the sensitivity towards glucose detection. However, if more than 20 seconds of deposition is applied under the conditions described here, the result is a decrease in sensitivity associated with the shape of the observed oxidation feature. It is therefore critical to utilize the optimized deposition process in order to achieve maximum sensor performance. This is clearly demonstrated in the results presented here, which are based on a simple, cheap and rapid method for the preparation of high performance biosensors for glucose electro-oxidation.

Table 2. A comparison of the performances of the BA5 and BA10-CuFoam biosensors with other copper and array based non-enzymatic glucose biosensors

Electrode	Potential (V)	Linear range	Sensitivity	Ref.
CuO@Cu nanowires array	+0.65 vs. Ag/AgCl	$1.0\text{x}10^{-6}$ – $1.0\text{x}10^{-2}$ M	1250.8 µA mM^{-1} cm^{-2}	[40]
Cu(OH)2 NGA@NPC hybrid	+0.52 vs. Ag/AgCl	0.2 – 9 mM	2.09 mA cm^{-2} mM^{-1},	[41]
Cu2O/MoS2	+0.7 vs Hg/Hg_2Cl_2	0.01–4 mM	3108.08 µA mM^{-1} cm^{-2}	[42]
CuO-ZnO NRs	+ 0.62 vs. Ag/AgCl	Up to 8.45 mM	2961.7 µA mM^{-1} cm^{-2}	[43]
Cu2O PLNWs/Cu foam	+0.5 vs. SCE	0.001–1.8 mM	6.6807 mA M^{-1} cm^{-2}	[44]
Cu/graphene/NF	+0.6 vs. Ag/AgCl	Linear response range of 100 µM	7.88 mA mM^{-1} cm^{-2}	[45]
Micro-Pt/Cu NFs/nafion/GOD/PU	+0.6 vs. Ag/AgCl	0 – 20 mM	42.38 nA mM^{-1}	[46]
Co_3O_4 nanosheets	+0.5 vs Ag/AgCl	Up to 0.31 mM	12.97 mA mM^{-1} cm^{-2}	[47]
Helical Cu_2O/TiO_2 nanotubes array	+0.65 vs. SCE	3 - 9 mM	14.56 µA mM^{-1} cm^{-2}	[48]
Hierarchical Co_3O_4/Ni	+0.5 vs. SCE	0.04 – 3.6 mM	13,855 µA mM^{-1} cm^{-2}	[49]
CuFoam/BA10	+0.45 vs. Ag/AgCl	0.01 - 22.55 mM	4,437 µA mM^{-1} cm^{-2}	This work
CuFoam/BA5	+0.45 vs. Ag/AgCl	0.01 - 22.55 mM	10,630 µA mM^{-1} cm^{-2}	This work

The selectivity of the sensors was studied in the presence of ascorbic acid, uric acid and acetaminophen, which can possibly coexist with glucose in human blood. Considering that the concentration of glucose in the human blood is more than 30 times that of the interfering species, the experiments designed to test the robustness of the electrodes towards these potential interfering species interference were conducted at both BA5 and BA10-CuFoam biosensors by making a series of additions of 1 mM glucose and 0.1 mM

interfering species into the electrochemical cell[48]. **Fig. S3A and B** shows the chronoamperograms of BA5 and BA10 recorded in response to each addition of glucose, ascorbic acid, uric acid, acetaminophen and glucose, respectively. The response of the glucose in the presence of interfering species showed a 5.8 % increase in the case of BA5 and a 3.1 % decrease in the case of BA10 (**Fig. 8A**).

It is therefore concluded that the very small changes of the measured responses resulting from the addition of the interfering species clearly demonstrate the selectivity of the developed biosensors towards glucose. The other significant effect to consider when using noble metal-based electrochemical biosensors is the possible poisoning of the surface by chloride ions, which are abundant in physiological fluids. For this reason we also studied the performance of the biosensors developed here in response to serial additions of 1 mM glucose into electrochemical cell in the absence and presence of 0.1 M NaCl. **Fig. 8B** shows the corresponding linear responses of both the BA5 and BA10 electrodes. The slopes of the BA5 and BA10 calibration curves in 0.1 M NaOH are 11,740 µA mM^{-1} cm^{-2} and 4,772 µA mM^{-1} cm^{-2}, respectively. Interestingly, the slope of BA5 and BA10 electrode calibration curves in a solution of 0.1 M NaOH containing 0.1 M NaCl are 12,610 µA mM^{-1} cm^{-2} and 5,016 µA mM^{-1} cm^{-2} respectively. The changes calculated are some 7.4 % for BA5 and 5.1 % for BA10 in the presence of the chloride ions.

These results demonstrate that the biosensors developed here not greatly perturbed by possible poisoning by chloride ions.

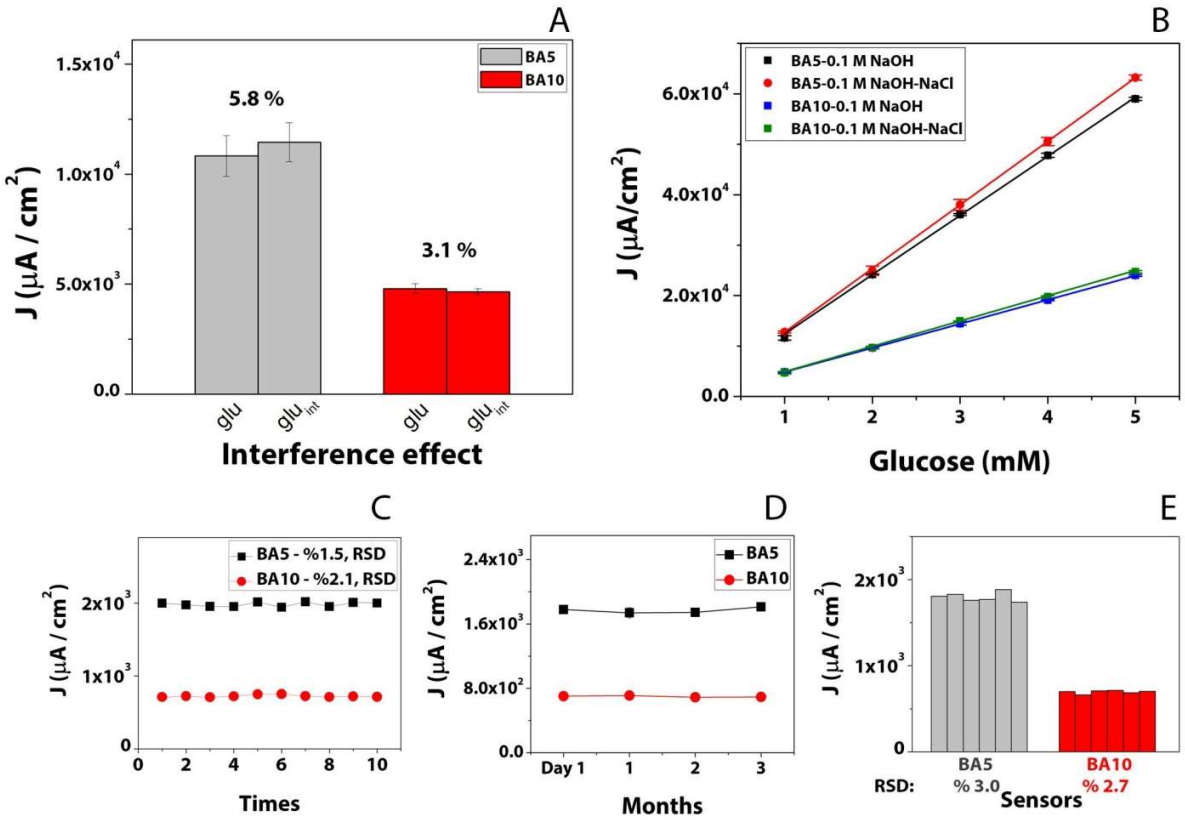

Figure 8. Interference effect (A), Poisoning effect (B), reusability (C), long term stability (D) and reproducibility (E) of BA5-CuFoam and BA10-CuFoam biosensors

The reusability of the biosensors was studied to investigate their operational stability.. The biosensors were examined 10 times in terms of their response towards 0.15 mM glucose and the resulting current densities are shown in **Fig. 8C**. The calculated relative standard deviations of the results from the BA5 and

BA10 electrodes within 10 consecutive experiments are 1.5 % and 2.1 %, respectively. Thus it may be seen that both biosensors exhibited excellent operational stability.

The long term stabilities of both biosensors were also tested over a period of three months. **Fig. 8D** shows the corresponding current densities recorded towards glucose every 30 days. The biosensors were then stored at room temperature in the dark when not in use. The current density of the BA5 electrode measured on the first day increased 1.9 % and the current density of the BA10 electrode decreased 1.35 % after three months. These negligible changes in the responses towards 0.15 mM glucose after three months suggest that both biosensors showed excellent long-term stabilities. The reproducibility of both the BA5 and BA10 electrodes are shown in **Fig. 8E**. Six as-prepared samples of BA5 were tested towards glucose by applying chronoamperometry and the relative standard deviation of the recorded current densities was calculated to be 3.0 % for BA5. Similarly, six BA10 biosensors were measured at the same conditions. The calculated relative standard deviation in this case was found to be 2.7 %. These statistics demonstrate the high degree of reproducibility associated with both the BA5 and BA10 biosensors.

Table3. Real sample analysis with spiked sterile human serum

		BA5-CuFoam biosensor		**BA10-CuFoam biosensor**	
Sample	**Spiked serum (mM)**	**Measured (mM)**	**Recovery (%)**	**Measured (mM)**	**Recovery (%)**
1	4.4	4.7 (± 0.04)	105.7	5.0 (± 0.07)	112.4
2	6.1	6.2 (± 0.06)	101.2	6.6 (± 0.29)	108.6
3	10	9.8 (± 0.35)	97.7	10.4 (± 0.15)	103.6

Finally, we have used the two biosensors developed here for the detection of glucose in sterile human serum. Four different spiked sterile human serum samples were prepared; 4.4, 6.1 and 10 mM. Each spiked serum concentration was studied three times and after each addition of the prepared sample into electrochemical cell, the current responses were recorded at +0.45 V vs. Ag/AgCl. By substituting the resulting current values into the calibration curves of the biosensors, the concentrations of the samples were calculated and the corresponding results are shown in **Table 3**. The recovery values of the BA5 electrode are in the range of 97.7 - 105.7 %. The recovery values of the BA10 electrode are in the range of 103.6 - 112.4 %. These results show that the developed BA5 and BA10-CuFoam biosensor electrodes can successfully determine the glucose concentrations in human serum.

4. Conclusions

In summary, two different band array electrodes were designed. Both designs had 17 band electrodes, 100 μm inter electrode distance and 200 nm recess depth. Silicon based micro band array electrodes, namely BA5 (with 5 μm width and 250 μm length) and BA10 (with 10 μm width and 500 μm length) were fabricated by applying microfabrication technologies including lithography, deposition and etching. The fabrication technologies used permit the precise and reproducible fabrication of electrodes using methods which are proven to be cost-effective for the batch production of devices. Scanning electron microscopy and electrochemistry were used for characterization of the bare electrodes. The fabricated electrodes were then used as substrates for Cu dendrites deposition at high negative overpotentials in an acidic environment. We observed that the increased acidity of the electrodeposition solution gave rise to a significant improvement in terms of the morphology and adhesion of the deposits. The CuFoam deposited band array electrodes were used as high performance electro catalysts for glucose detection. While both designs showed excellent electrocatalytic activity towards glucose, the BA5-CuFoam biosensor

in particular exhibited an outstanding sensitivity of 10,630 μA mM^{-1} cm^{-2} with a wide concentration range of 0.01 mM – 22.55 mM. This result is one of the highest sensitivity ever recorded among the non-enzymatic glucose biosensors reported up to now in the literature. Furthermore, both developed biosensors showed a strong resistance to the poisoning effects of chloride ions while also exhibiting excellent reproducibility, reusability, and negligible interference effects in the presence of ascorbic acid, uric acid and acetaminophen. The electrodes and biosensors described in this work are suitable for further miniaturization and packaging. Moreover, this study shows the promising advantages of the foam modified array electrodes in terms of the stability, increased electroactive surface area and analytical performance.

Methods:

Chemicals and instrumentation. Copper(II) chloride dihydrate ($CuCl_2 \cdot 2H_2O$), glucose, ascorbic acid, uric acid, acetaminophen, potassium ferrocyanide ($K_4[Fe(CN)_6]$), potassium ferricyanide ($K_3[Fe(CN)_6]$), uric acid, acetaminophen, phosphate buffer saline tablets (PBS, 0.01 M, pH7.4), sodium hydroxide (NaOH), sulfuric acid and potassium chloride were obtained from Sigma-Aldrich. All solutions were prepared with double distilled 18.3 MΩ deionized water which was obtained by ELGAPurelab Ultra. Electrochemical measurements were performed on an Autolab electrochemical workstation (Metrohm, UK) equipped with a conventional 3-electrode setup consisting of a micro band array electrode (working electrode, see fabrication below), a spiral Pt wire counter electrode and Ag/AgCl (1 M KCl) reference electrode. The surface morphology and the nanostructure of the bare and modified electrodes was studied by scanning electron microscopy (SEM) (Zeiss Supra 40 SEM at accelerating voltages in the range of 5-10 kV). The chemical composition of the surface was characterized by using an X-ray photoemission spectrometer (XPS, Kratos AXIS ULTRA) with Al K_α at 1486.58 eV. All the XPS data were calibrated by the carbon 1s peak at 284.8 eV. The energy dispersive X-ray analyses (EDX) was studied by using SEM Quanta 650 Field Emission Gun (FEG) attached with EDX unit, with accelerating voltage of 20 kV.

Microfabrication of electrodes. Silicon-based gold array electrodes were fabricated by a general microfabrication flow which included lithography, deposition and etching as we reported earlier [8,9]. The masks consisted of a series of the array geometries required were designed specifically for band array fabrication. In the first step of the fabrication process, a silicon oxide layer was grown on the silicon substrate followed by spin coating of a photoresist. The metal layers - titanium first and then gold - were deposited and patterned by a lift-off process. A 200 nm thick silicon nitride layer was deposited as the passivation layer. Finally the mask was used for a passivation lithography process and the etching of the arrays and contact pad. The overall wafer was covered with a resist layer to protect the electrodes during dicing.

Electrochemical measurements and CuFoam electrode preparation. All electrochemical experiments were performed at room temperature, in 5mL total electrolyte volume. Prior to each electrochemical study, electrodes were treated with organic solvents and plasma cleaned to remove the resist layer. Firstly, electrodes were kept in hot acetone (56°C; boiling point) for 3 minutes and then rapidly transferred into isopropyl alcohol and treated in an ultrasonic bath for 3 minutes. After the organic solvent cleaning process, the electrodes were washed with deionized water and dried under nitrogen flow. Dry electrodes were placed into the plasma cleaner to increase the hydrophilicity of the surface and remove the organic residues or oxides from the surface. Electrodes were then washed with deionized water and dried under N_2 flow. The clean electrodes were then used immediately.

Cyclic voltammetry of the bare electrodes was typically performed at a scan rate of 0.01 V s^{-1}, in a stationary solution of 5 mM $[Fe(CN)_6]^{3-/4-}$ prepared in 0.01 M PBS (pH 7.4), containing 0.1 M KCl. Electrodeposition of copper was carried out by applying chronoamperometry in 6mL 2.5 M H_2SO_4 solution

containing 0.87 mg Cu^{2+} with suitable applied voltage and time for each design. Prior to each electrodeposition process electrochemical cell was pre-conditioned for 2 seconds at 0 V. Band array 5 (BA5) with 5 µm width, 250 µm length was applied **-5 V for 20 seconds.** Band array 10 (BA10) with 10 µm width, 500 µm length was studied at **-6 V for 25 seconds.** Both band arrays have 17 electrodes. Both electrodes have 200 nm recess depth. After deposition, the CuFoam electrodes were rinsed with double distilled water and dried in air. Cyclic voltammetry of CuFoam deposited microelectrodes was performed in alkaline media, 0.1 M NaOH at a scan rate of 0.01 V s^{-1} in the absence and presence of glucose. Oxidation of the glucose was firstly studied by linear sweep voltammetry (LSV) at a scan rate of 0.01 V s^{-1}. Calibration of glucose sensors was prepared by measuring the chronoamperometric response at the 40^{th} second of applied potential of +0.45 V in 0.1 M NaOH solution. Firstly, electrodes were studied in the absence of glucose to determine the base current value at 40^{th} second. After addition of the glucose the current value was obtained at 40^{th} second under the same conditions used for the base study and the difference between the values was taken as an analytical signal. All sensitivities were determined by dividing the slope of the calibration curves by total geometric surface area of each array electrode.

Acknowledgments
The authors gratefully acknowledge the support of the Department of Agriculture, Food and the Marine in Ireland, via award number 14F883 .

References.

1 Fekete, Z. Recent advances in silicon-based neural microelectrodes and microsystems: a review. *Sensors and Actuators B: Chemical* **215**, 300-315, doi:https://doi.org/10.1016/j.snb.2015.03.055 (2015).

2 Seymour, J. P., Wu, F., Wise, K. D. & Yoon, E. State-of-the-art MEMS and microsystem tools for brain research. *Microsyst Nanoeng* **3**, doi:10.1038/micronano.2016.66 (2017).

3 Pongrácz, A. *et al.* Deep-brain silicon multielectrodes for simultaneous in vivo neural recording and drug delivery. *Sensors and Actuators B: Chemical* **189**, 97-105, doi:https://doi.org/10.1016/j.snb.2013.01.032 (2013).

4 Day, B. K., Pomerleau, F., Burmeister, J. J., Huettl, P. & Gerhardt, G. A. Microelectrode array studies of basal and potassium-evoked release of L-glutamate in the anesthetized rat brain. *J Neurochem* **96**, 1626-1635, doi:10.1111/j.1471-4159.2006.03673.x (2006).

5 Kane, S. R. *et al.* Electrical Performance of Penetrating Microelectrodes Chronically Implanted in Cat Cortex. *Ieee T Bio-Med Eng* **60**, 2153-2160, doi:10.1109/Tbme.2013.2248152 (2013).

6 Fekete, Z., Németh, A., Márton, G., Ulbert, I. & Pongrácz, A. Experimental study on the mechanical interaction between silicon neural microprobes and rat dura mater during insertion. *Journal of Materials Science: Materials in Medicine* **26**, 70, doi:10.1007/s10856-015-5401-y (2015).

7 Wei, W. *et al.* An implantable microelectrode array for simultaneous L-glutamate and electrophysiological recordings in vivo. *Microsystems &Amp; Nanoengineering* **1**, 15002, doi:10.1038/micronano.2015.2 https://www.nature.com/articles/micronano20152#supplementary-information (2015).

8 Buk, V. & Pemble, M. E. A highly sensitive glucose biosensor based on a micro disk array electrode design modified with carbon quantum dots and gold nanoparticles. *Electrochimica Acta* **298**, 97-105, doi:https://doi.org/10.1016/j.electacta.2018.12.068 (2019).

9 Buk, V., Pemble, M. E. & Twomey, K. Fabrication and evaluation of a carbon quantum dot/gold nanoparticle nanohybrid material integrated onto planar micro gold electrodes for potential

bioelectrochemical sensing applications. *Electrochimica Acta* **293**, 307-317, doi:10.1016/j.electacta.2018.10.038 (2019).

10 Patolsky, F., Zheng, G. & Lieber, C. M. Fabrication of silicon nanowire devices for ultrasensitive, label-free, real-time detection of biological and chemical species. *Nat Protoc* **1**, 1711-1724, doi:10.1038/nprot.2006.227 (2006).

11 Yang, N., Uetsuka, H., Osawa, E. & Nebel, C. E. Vertically aligned diamond nanowires for DNA sensing. *Angew Chem Int Edit* **47**, 5183-5185, doi:10.1002/anie.200801706 (2008).

12 Siddiqui, S., Arumugam, P. U., Chen, H., Li, J. & Meyyappan, M. Characterization of Carbon Nanofiber Electrode Arrays Using Electrochemical Impedance Spectroscopy: Effect of Scaling Down Electrode Size. *Acs Nano* **4**, 955-961, doi:10.1021/nn901583u (2010).

13 Arumugam, P. U. *et al.* Wafer-scale fabrication of patterned carbon nanofiber nanoelectrode arrays: A route for development of multiplexed, ultrasensitive disposable biosensors. *Biosensors and Bioelectronics* **24**, 2818-2824, doi:https://doi.org/10.1016/j.bios.2009.02.009 (2009).

14 Xie, L., Asiri, A. M. & Sun, X. Monolithically integrated copper phosphide nanowire: An efficient electrocatalyst for sensitive and selective nonenzymatic glucose detection. *Sensors and Actuators B: Chemical* **244**, 11-16, doi:https://doi.org/10.1016/j.snb.2016.12.093 (2017).

15 Xie, F., Cao, X., Qu, F., Asiri, A. M. & Sun, X. Cobalt nitride nanowire array as an efficient electrochemical sensor for glucose and H2O2 detection. *Sensors and Actuators B: Chemical* **255**, 1254-1261, doi:https://doi.org/10.1016/j.snb.2017.08.098 (2018).

16 Li, Y. *et al.* Porous NiTe2 nanosheet array: An effective electrochemical sensor for glucose detection. *Sensors and Actuators B: Chemical* **274**, 427-432, doi:https://doi.org/10.1016/j.snb.2018.07.172 (2018).

17 Xie, F., Liu, T., Xie, L., Sun, X. & Luo, Y. Metallic nickel nitride nanosheet: An efficient catalyst electrode for sensitive and selective non-enzymatic glucose sensing. *Sensors and Actuators B: Chemical* **255**, 2794-2799, doi:https://doi.org/10.1016/j.snb.2017.09.095 (2018).

18 Gawande, M. B. *et al.* Cu and Cu-Based Nanoparticles: Synthesis and Applications in Review Catalysis. *Chemical Reviews* **116**, 3722-3811, doi:10.1021/acs.chemrev.5b00482 (2016).

19 Koepke, S. J., Light, K. M., VanNatta, P. E., Wiley, K. M. & Kieber-Emmons, M. T. Electrocatalytic Water Oxidation by a Homogeneous Copper Catalyst Disfavors Single-Site Mechanisms. *J Am Chem Soc* **139**, 8586-8600, doi:10.1021/jacs.7b03278 (2017).

20 Bae, K. L., Kim, J., Lim, C. K., Nam, K. M. & Song, H. Colloidal zinc oxide-copper(I) oxide nanocatalysts for selective aqueous photocatalytic carbon dioxide conversion into methane. *Nat Commun* **8**, doi:10.1038/s41467-017-01165-4 (2017).

21 Buk, V., Emregul, E. & Emregul, K. C. Alginate copper oxide nano-biocomposite as a novel material for amperometric glucose biosensing. *Mat Sci Eng C-Mater* **74**, 307-314, doi:10.1016/j.msec.2016.12.003 (2017).

22 Tian, K., Prestgard, M. & Tiwari, A. A review of recent advances in nonenzymatic glucose sensors. *Mat Sci Eng C-Mater* **41**, 100-118, doi:10.1016/j.msec.2014.04.013 (2014).

23 Jiang, J. Y., Zhang, P., Liu, Y. & Luo, H. X. A novel non-enzymatic glucose sensor based on a Cu-nanoparticle-modified graphene edge nanoelectrode. *Anal Methods-Uk* **9**, 2205-2210, doi:10.1039/c7ay00084g (2017).

24 Cao, F. & Gong, J. Nonenzymatic glucose sensor based on CuO microfibers composed of CuO nanoparticles. *Anal Chim Acta* **723**, 39-44, doi:10.1016/j.aca.2012.02.036 (2012).

25 Fang, L. X. *et al.* Flower-like MoS2 decorated with Cu2O nanoparticles for non-enzymatic amperometric sensing of glucose. *Talanta* **167**, 593-599, doi:10.1016/j.talanta.2017.03.008 (2017).

26 Zhao, Y. X., Li, Y. P., He, Z. Y. & Yan, Z. F. Facile preparation of Cu-Cu2O nanoporous nanoparticles as a potential catalyst for non-enzymatic glucose sensing. *Rsc Adv* **3**, 2178-2181, doi:10.1039/c2ra22654e (2013).
27 Nam, D. H., Taitt, B. J. & Choi, K. S. Copper-Based Catalytic Anodes To Produce 2,5-Furandicarboxylic Acid, a Biomass-Derived Alternative to Terephthalic Acid. *Acs Catal* **8**, 1197-1206, doi:10.1021/acscatal.7b03152 (2018).
28 Nam, D. H. & Choi, K. S. Bismuth as a New Chloride-Storage Electrode Enabling the Construction of a Practical High Capacity Desalination Battery. *J Am Chem Soc* **139**, 11055-11063, doi:10.1021/jacs.7b01119 (2017).
29 Nikolić, N. D., Branković, G., Pavlović, M. G. & Popov, K. I. The effect of hydrogen co-deposition on the morphology of copper electrodeposits. II. Correlation between the properties of electrolytic solutions and the quantity of evolved hydrogen. *J Electroanal Chem* **621**, 13-21, doi:https://doi.org/10.1016/j.jelechem.2008.04.006 (2008).
30 Cherevko, S. & Chung, C.-H. Direct electrodeposition of nanoporous gold with controlled multimodal pore size distribution. *Electrochemistry Communications* **13**, 16-19, doi:https://doi.org/10.1016/j.elecom.2010.11.001 (2011).
31 Caballero-Briones, F., Artes, J. M., Diez-Perez, I., Gorostiza, P. & Sanz, F. Direct Observation of the Valence Band Edge by in Situ ECSTM-ECTS in p-Type Cu2O Layers Prepared by Copper Anodization. *J Phys Chem C* **113**, 1028-1036, doi:10.1021/jp805915a (2009).
32 El Din, A. M. S. & El Wahab, F. M. A. The behaviour of the copper electrode in alkaline solutions upon alternate anodic and cathodic polarization. *Electrochimica Acta* **9**, 113-121, doi:https://doi.org/10.1016/0013-4686(64)80010-4 (1964).
33 Hampson, N. A., Lee, J. B. & Macdonald, K. I. Oxidations at copper electrodes: Part 2. a study of polycrystalline copper in alkali by linear sweep voltammetry. *Journal of Electroanalytical Chemistry and Interfacial Electrochemistry* **32**, 165-173, doi:https://doi.org/10.1016/S0022-0728(71)80183-3 (1971).
34 Deng, Y. L., Handoko, A. D., Du, Y. H., Xi, S. B. & Yeo, B. S. In Situ Raman Spectroscopy of Copper and Copper Oxide Surfaces during Electrochemical Oxygen Evolution Reaction: Identification of Cu-III Oxides as Catalytically Active Species. *Acs Catal* **6**, 2473-2481, doi:10.1021/acscatal.6b00205 (2016).
35 Zheng, W. R. *et al.* Cu-II-Mediated Ultra-efficient Electrooxidation of Glucose. *Chemelectrochem* **4**, 2788-2792, doi:10.1002/celc.201700712 (2017).
36 Miller, B. Split-Ring Disk Study of Anodic Processes at a Copper Electrode in Alkaline Solution. *J Electrochem Soc* **116**, 1675-&, doi:Doi 10.1149/1.2411657 (1969).
37 Toghill, K. E. & Compton, R. G. Electrochemical Non-enzymatic Glucose Sensors: A Perspective and an Evaluation. *Int J Electrochem Sc* **5**, 1246-1301 (2010).
38 Kano, K., Takagi, K., Inoue, K., Ikeda, T. & Ueda, T. Copper electrodes for stable subpicomole detection of carbohydrates in high-performance liquid chromatography. *J Chromatogr A* **721**, 53-57, doi:https://doi.org/10.1016/0021-9673(95)00757-1 (1996).
39 Kano, K., Torimura, M., Esaka, Y., Goto, M. & Ueda, T. Electrocatalytic oxidation of carbohydrates at copper(II) -modified electrodes and its application to flow-through detection. *J Electroanal Chem* **372**, 137-143, doi:https://doi.org/10.1016/0022-0728(93)03252-K (1994).
40 Dong, J. *et al.* Direct electrodeposition of cable-like CuO@Cu nanowires array for non-enzymatic sensing. *Talanta* **132**, 719-726, doi:https://doi.org/10.1016/j.talanta.2014.10.027 (2015).
41 Li, R., Liu, X., Wang, H., Wu, Y. & Lu, Z. High-performance hybrid electrode decorated by well-aligned nanograss arrays for glucose sensing. *Biosensors and Bioelectronics* **102**, 288-295, doi:https://doi.org/10.1016/j.bios.2017.11.007 (2018).

42 Fang, L. *et al.* Flower-like MoS2 decorated with Cu2O nanoparticles for non-enzymatic amperometric sensing of glucose. *Talanta* **167**, 593-599, doi:https://doi.org/10.1016/j.talanta.2017.03.008 (2017).

43 Ahmad, R. *et al.* Highly Efficient Non-Enzymatic Glucose Sensor Based on CuO Modified Vertically-Grown ZnO Nanorods on Electrode. *Sci Rep-Uk* **7**, doi:10.1038/s41598-017-06064-8 (2017).

44 Lu, W. *et al.* Direct growth of pod-like Cu2O nanowire arrays on copper foam: Highly sensitive and efficient nonenzymatic glucose and H2O2 biosensor. *Sensors and Actuators B: Chemical* **231**, 860-866, doi:https://doi.org/10.1016/j.snb.2016.03.058 (2016).

45 Hussain, S. *et al.* A highly sensitive enzymeless glucose sensor based on 3D graphene-Cu hybrid electrodes. *New J Chem* **39**, 7481-7487, doi:10.1039/c5nj01512j (2015).

46 Fang, Y. *et al.* Development of Cu nanoflowers modified the flexible needle-type microelectrode and its application in continuous monitoring glucose in vivo. *Biosensors and Bioelectronics* **110**, 44-51, doi:https://doi.org/10.1016/j.bios.2018.03.024 (2018).

47 Meng, S. J. *et al.* Cobalt oxide nanosheets wrapped onto nickel foam for non-enzymatic detection of glucose. *Nanotechnology* **27**, doi:10.1088/0957-4484/27/34/344001 (2016).

48 Long, M., Tan, L., Liu, H., He, Z. & Tang, A. Novel helical TiO2 nanotube arrays modified by Cu2O for enzyme-free glucose oxidation. *Biosensors and Bioelectronics* **59**, 243-250, doi:https://doi.org/10.1016/j.bios.2014.03.032 (2014).

49 Xu, H. *et al.* Electrochemical non-enzymatic glucose sensor based on hierarchical 3D Co3O4/Ni heterostructure electrode for pushing sensitivity boundary to a new limit. *Sensors and Actuators B: Chemical* **267**, 93-103, doi:https://doi.org/10.1016/j.snb.2018.04.023 (2018).